A Complete Frequency Response Service Scheme using PV-Supercapacitor Cascade Topology

Sivakrishna Karpana
Department of Electrical Engineering
IIT Kharagpur
Kharagpur, India
karpanasivakrishna@gmail.com

Efstratios Batzelis
School of Electronic and Computer Science
University of Southampton
Southampton, UK
e.batzelis@soton.ac.uk

Suman Maiti
Department of Electrical Engineering
IIT Kharagpur
Kharagpur, India
sumanmaiti@gmail.com

Chandan Chakraborty
Department of Electrical Engineering
IIT Kharagpur
Kharagpur, India
chakraborty@ieee.org

***Abstract*—Frequency response services have become more important than ever in an increasingly inertia-less power system. A promising way to provide such services in a photovoltaic (PV) system is by hybridizing with supercapacitors (SC) due to their high power density, long operating cycles and fast response. The challenge, however, with a PV/SC system is what topology can effectively integrate such devices with so low and variable voltage, as well as how to control them for optimal utilization of their very limited capacity. This paper builds upon a previously introduced PV/SC cascade topology and proposes a complete control scheme for frequency services. A power segregation mechanism infers how the power demand is shared between SC and PV array, accounting for the operational boundaries of the former and occasionally deciding short-term curtailments for the latter. The proposed scheme involves also a voltage recovery function to slowly get the SC voltage back to the steady-state value after a disturbance, the latter being calculated via a newly introduced methodology. MATLAB/Simulink simulations validate the control efficacy under a series of frequency disturbances.**

Keywords— Frequency Response, Supercapacitor, Synthetic Inertia, Inertial Response, Primary Frequency Response, PV systems, PV SC Cascade Topology.

I. INTRODUCTION

In classical Power System (PS), the Inertia Response (IR) is intrinsic due to the stored kinetic energy in their rotating mass. This, although temporary, helps limiting the initial Rate of Change of Frequency (RoCoF). later assisted by a slower governor response to contain the frequency drop within the set limits and eventually restore it to the nominal levels with time. However, increasing deployment of Photovoltaic Systems (PVS) and other inverter-based resources is making the PS more vulnerable even to a small disturbance leading to a large frequency fluctuation. It is due to steady drop in the equivalent system inertia [1]. It may sometimes trigger snow bowling phenomena of cascaded load disconnection in case the frequency fluctuation exceeds certain standard boundaries set by the grid operators. In the past, many such cases made the news in various places of the world with complete black out for hours [2]-[4]. Those instances were because of either high Rate of Change of Frequency (RoCoF), longer frequency event or deeper frequency nadir resulting in inconvenience for millions of people.

Estimations forecast that, by the end of 2022, Indian will see almost 22% fall in the total system inertia [2]. Therefore, it is the peak time to find an appropriate yet handy solution to emulate Synthetic Inertia (SI) in PVS to safeguard the stability of the PS. For this, it is essential for the PVS to have some kind of embedded storage to emulate similar or even better IR like synchronous machines. Different kind of storage devices and their hybridization with PV for such applications have been cited in literature [6]-[11]. In [6], [7], the benefits of Superconductive Magnetic Energy Storage (SMES) have been explored; whereas, in [8], [9], the advantages of Battery Energy Storage (BES) over SMES has been highlighted. On the contrary, few literature talks about the benefits of hybrid ES over BES/SMES. In [10], the PV-Flywheel hybridization helps in SI emulation by using the stored mechanical inertia of the flywheel. Similarly in [11] a PV-Diesel-Fuel Cell based hybrid ES and its advantages has been explored.

In recent past, the use of electric double layer capacitor/ ultra-capacitor, also known as Supercapacitor (SC), has been gaining popularity among the other ESs due to its faster response, impulse power handling capability, long operating cycle and much smaller footprint etc. However, due to low energy density, it is often used along with other storage classes like BES [12] or fuel cell [13] mostly for high energy and power intensive services. It has been a debatable topic on how to integrate SC storage to PVS. The very basic way could be just connecting the SC to the main DC link and then extract energy via energy extraction schemes cited in [14], [15]; however, that would require a very large SC with minimum utilization factor as we cannot fluctuate the DC link voltage much.

Therefore, selection of a proper interfacing converter is very vital for PV-SC hybridization. The most common parallel configurations with isolated converter still may not be a good choice here due to limited gain issues as SC voltage greatly varies with SOC [16]. In addition, high-gain isolated converters suffer from lower reliability and increased system complexity. Recently, a new PV/SC Cascade Topology (PSCT) [16] is reported in the literature, which finds a way out to integrate a very low voltage SC unit to PVS in a kind of series connection without the need of high gain interfacing converters. However, the reported control scheme is only for SI Response (SIR) for a Continuous Frequency Fluctuation (CFF) and a part of a Primary Frequency Response (PFR) i.e. Under Frequency Event (UFE). There is no scope for Over Frequency Event (OFE) due to limited storage capability.

Some literature talks about the concept of Virtual Energy Storage (VES), where a portion of PV array's capacity as active power storage is intentionally kept as reserve or switch to reserve mode when necessary. This concept is also known as PV reserves, power headroom or PV delta power control method [17]-[20] mostly suitable for Frequency Response Services (FRS). The researchers in [17] actually use a multi-string approach, where they operate one string dedicatedly at Maximum Power Point Tracking (MPPT) mode to extract the real time MPPT information, which they use for the other strings to operate in Power Curtailment Control (PCC) mode

just by subtracting the required delta amount of power. However, this results in low PV voltage due to left hand side operation of the PV characteristics. In [18], the control switches between MPPT mode and PCC mode when necessary but operates in the right hand side of the PV characteristics to avoid low PV voltage problem. However, it suffers from no room for extra power delivery during an UFE when in MPPT mode. The work in [19] continuously operates at deloaded power point to provide reserve in the system so that both positive and negative power demand can be met; however, it suffers from underutilization of the PV capacity. Similar works are also done in [20] but for grid forming control which is not in the focus of our work.

The research gap and the problem statement picked up as challenge through this article are highlighted below with appropriate solution:

- Firstly, until date, no such work has been cited in the literature, which takes the benefit of both SC storage and PCC addressing a complete FRS scheme for a PVS. To address this, here the authors have picked up the PSCT topology in [16] as a best approach for aiming SIR and the FRS during an UFE along with the PCC scheme in [18] to target the FRS during an OFE. The idea is to target a complete, yet energy efficient, FRS scheme for the best possible uses of both SC and PV by optimally sharing the power profile between them.
- Secondly, it is important to find a methodology to calculate the optimal voltage set point at Steady State (SS) to address both SIR and UFE optimally without the need of strict frequency information.
- Thirdly, a slow Voltage Recovery Scheme (VRS) should always be running in the background to ensure the SS voltage for the SC at any point of time, which is often over looked in literature.
- Fourthly, alongside, a Voltage Protection Scheme (VPS) is indeed essential to safeguards the extreme voltage limits of the SC without interfering with the VRS.

The paper is organized into the following sections. Section II gives detailed background information/considerations for this paper, followed by Section III, which explains the proposed control scheme. In Section IV, the methodology for calculating the SS voltage set point is covered. The idea is validated via MATLAB/Simulink simulations in Section V. Eventually, Section VI concludes the paper.

II. Background Work

A. PVS Under Considertion

This sub-section covers the briefly the PVS under consideration, the targeted FRSs with benchmark parameters as shown in Table 1. A medium power level PV string inverter system for roof top application with inbuilt IR characteristics is the centre of attention here.

B. PSCT and Working Principle

This sub section talks about the targeted PV-SC Cascade Topology, a good option for PV-SC hybridization without the need for a high-gain converter. The circuit configuration of the PSCT is shown in the Fig. 1. As depicted in [16], the SC and the associated Power Conversion Stages (PCS) can be

TABLE I. System under Consideration

System Under Consideration	Parameters and values		
PV system	DC side	10 kWp, 495V & 20A @ STC DC link voltage 700V	
	AC side	400 Vrms & 50 Hz	
For Synthetic Inertia Response	Maximum allowable frequency fluctuation		$\pm 0.0036\ PU \approx \pm 180 mHz$
	RoCoF		$\pm$0.3 Hz/sec
	Inertia Constant (H)		9 sec
For Primary Frequency Response	Dead band (db_{UF})		$\pm$0.003 (150 mHz/50 Hz)
	Droop coefficient (k_{UF})		12%
	Time of disturbance (t_{ini})		6.9 sec
	Duration of Fault (T_f)		16.1 sec
	Frequency nadir point (f_{nadir})		50 $\pm$ 0.55 Hz
	Frequency offset point (f_{offset})		50 $\pm$ 0.2 Hz
	Occurrence of f_{nadir} ($t_{f_{nadir}}$)		0.214 T_f

connected in series with the PV at the input side of the Boost converter meant for MPPT operation of the PVS. That means, the output port of the SC-PCS shares the common PV current tracked by the PV MPPT converter. The idea here is to operate the SC as a voltage source rather current source. Therefore, by simply regulating the output voltage of the SC-PCS with required magnitude and polarity, we can either charge or discharge the SC. This can be achieved by connecting a bidirectional buck-boost DC-DC converter followed by a Semi-controlled Inverter (SCI). The DC-DC stage is for boosting operation (2 to 5 times). Whereas, the SCI is a polarity changer and sometimes for bucking operation. Due to the series connection, it does not really matter what actually is the voltage of the SC while charging or discharging. Theoretically, it can be discharged fully to zero voltage unlike parallel configurations; however, it has a limitation in terms of current reflected at the SC end, thus, the power due to limited gain of the non-isolated DC-DC converter of the SC stage. The detailed description and the working principle of PSCT is explained in [16] and is beyond the scope of this paper.

Nevertheless, for the low-energy high-power requirements of FRS, the SC could be a cost-effective option to hybridize a PVS with the energy storage of required voltage and energy rating. Additionally, the PSCT topology passes all such requirements ideal for the integration of a low and variable voltage storage while delivering the FRS meant for PVS. Furthermore, due to series connection, the PV MPPT operation is also completely decoupled from the SC stage of

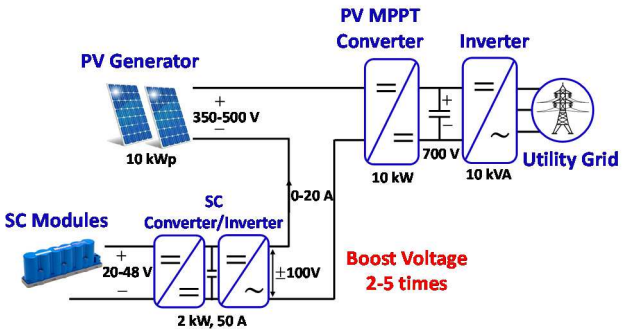

Fig. 1. The PV-SC Cascade Topology under consideration.

TABLE II. DESIGN SPECS UNDER CONSIDERATION

SC storage	Parameters and values
Model number	BMOD0058 E016 B02
Maximum power demand (P_{sc}^{max})	≈ 2 kW for UFE and ≈ 1.2 kW for SIR (nearly 20% of PV capacity)
Maximum energy demand (E_{sc}^{max})	≈ 14.2 kJ during UFE
Minimum voltage (V_{sc}^{min}) of the SC below which it should not be discharged	≈ 20 V (to limit worst case voltage gain around 2 to 5 times for the SC-PCS)
Peak current rating of the SC-PCS at the SC end (I_{sc}^{max})	≈ 50 Amp (which decides total minimum No. SC units required)
No of units SC required	Three Nos. connected in series with total capacity 22 kJ, 19.33 F, 48 V & 170 Amps (peak)
Maximum allowable voltage of the SC above which it should not be charged	≈ 48 V (hard voltage limit)

operation. This was possible as the dynamics of SC power and voltage variation are much slower than the PV MPPT dynamics. Hence, brought our attention towards it.

In [16], a detailed analysis is also carried out for the sizing of the SC unit while targeting the SIR during a CFF and PFR during an UFE for the benchmark parameters listed in Table I. The corresponding results are listed in Table II. Moreover, the same will be taken forward as a base in this paper for further analysis.

The only service the PSCT cannot provide using the same small storage is the PFR during an OFE. This research gap has been taken care of through the PV PCC scheme this paper, which will be explained in detail in the next section.

III. CONTROL SCHEME

This section gives a clear-cut idea about the implemented control scheme to provide an all-round FRS to a PVS through the adopted PSCT. A complete block diagram of the overall control is shown in Fig. 2. As can be depicted, it can be divided into five subsystems:

1. Power estimation logic for FRS
2. Zone wise SC voltage control logic
3. Power segregation logic for PV and SC
4. Seamless PV MPPT and PV PCC
5. SC power stage control

A. Power Estimation Logic for FRS

The power estimation logic for FRS block is a combined control scheme for both SIR and PFR. Here, the ΔP_{RoCoF} term can be calculated using the swing equation like synchronous generators and the ΔP_{Droop} term can be found using the standard droop control method [16]. The output of this block is the net power (ΔP_{FR}) required for the FRS operation of the PVS.

B. Zone wise SC Voltage Control Logic

Zone wise SC voltage control block plays a crucial role in managing the SC voltage independently of the FRS. It has two main parts: one is the SS-VRS and the second one is the VPS. The SS-VRS can be treated as the outermost loop with sufficiently large time constant to avoid interference with other PI controllers in the system. This helps in bringing the SC voltage back to its SS value at any point of time. It is a band pass type control, whose input is peak and tail shaved such that it is activated only for the range between V_{SC}^{min} and V_{SC}^{nom} to avoid interference with the VPS. Selection for (V_{SC}^{SS}) will be discussed in detail in the next section. The second part is VPS, which acts as a safeguard to the SC. It is a very fast control that is activated only when the voltage limits are hit i.e. V_{SC}^{min} and V_{SC}^{nom}. Then the sum of both i.e. ΔP_{SC}^{Rec} and ΔP_{SC}^{Clamp} act as feed forward term to ΔP_{FR} to decouple it from the FRS before feeding to the PSL control block.

C. Power Segregation Logic for PV and SC

The next part of the control is the Power Segregation Logic (PSL) control. The main concept here is to segregate the power between the PV and SC for FRS in such a way that an optimal use of the available resources can be obtained with zero/minimal involvement of PV based on the type of

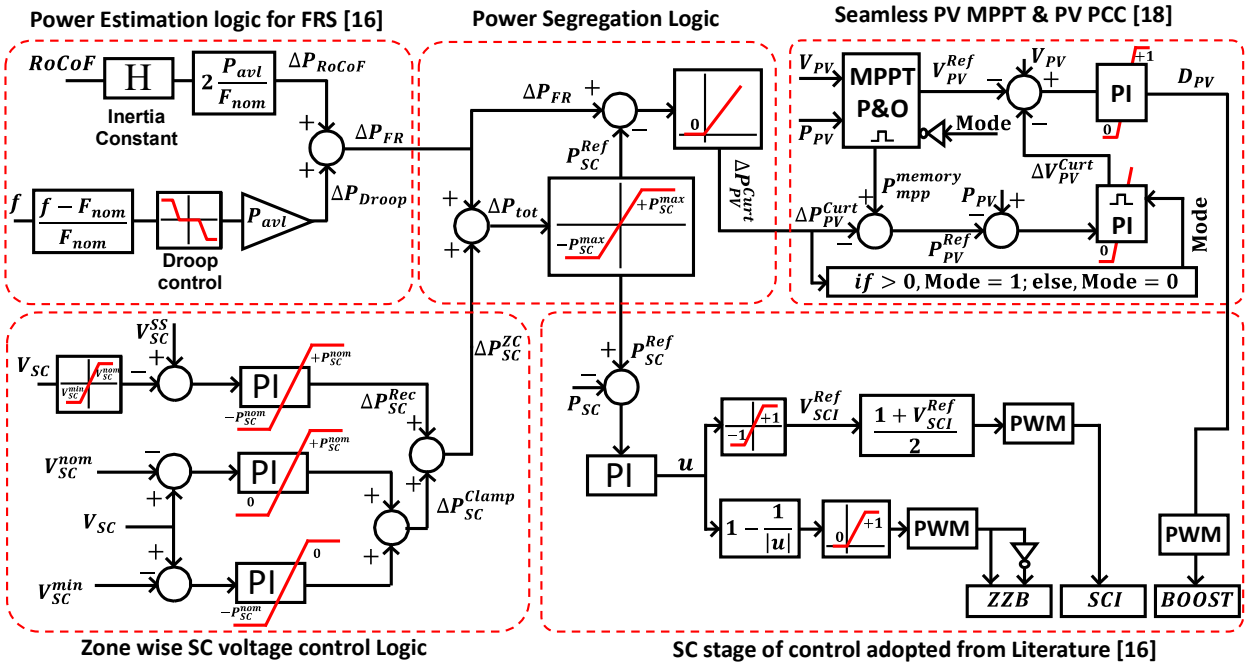

Fig. 2. Implemented control scheme to provide complete FRS to a PVS through the adopted PSCT.

frequency event. The idea is during a CFF and/or an UFE, discharge the stored energy of the SC to meet the power and energy demand (Anyways, we cannot extract more power from PV as it is already operating in MPPT mode). The benefit will be that we need not to operate the PV array in a pre-deloaded condition [17], [19] infinitely (reserves), saving a lot of energy out of it. However, during an OFE, the idea is to give the first priority to SC, let it charge until V_{SC}^{nom} (no worries, VPS will safe guard the SC), then the PSL control automatically transfers the remaining power as curtailment power command (ΔP_{PV}^{Curt}) to PV side control for curtailment. The VPS plays a vital role here to avoid an abrupt change in power command between SC and PV. In addition to that, the PSL control also take care of the P_{SC}^{max} limit irrespective of the type of the event, to avoid current overloading of the SC-PCS converters. The parameter P_{SC}^{max} is a variable quantity and can be calculated as in (1).

$$P_{SC}^{max} = |I_{SC}^{max}|V_{SC} \tag{1}$$

D. Seamless PV MPPT and PV PCC

The next part of the control is the PV side control. Here, based on the status of the ΔP_{PV}^{Curt} command, the control switches between the PV MPPT mode and the PV PCC mode seamlessly. Both the controls are enabled/disabled in a complementary fashion with commands when necessary, whose outputs freeze and reset respectively when disabled. Their outputs act as a feedforward term to either of the control schemes to have a seamless transition between them [18].

E. SC Power Stage Control

The control section ends with the final part of the control that is the SC-PCS control. As discussed in the previous section it consists of a DC-DC stage followed a semi-controlled inverter. Here a single PI controller generates the duty for the switches of the SC-PCS via a series of signal conditioning blocks [16]. For more details, please see [16].

IV. ESTIMATION OF SS VOLTAGE SET-POINT FOR SC

This section describes the methodology adopted here to calculate a SS voltage set point for the SC, which is mostly ignored in literature. This is very crucial for the point of view of the SC in order to calculate the minimum headroom required for an uncompromised SIR operation without involvement of the PV. This is not possible if the SC is fully charged to V_{SC}^{nom}.

Here, a very simple yet straightforward approach has been considered for the calculation of minimum headroom for SC. As discussed in [16], the SIR operation is mostly a power intensive service; however, the net energy demand is almost zero over a period of few tens of sec due to nearly uniform fluctuation of the frequency over the nominal value. However, the instantaneous energy demand is always a function of the instantaneous power demand. In addition, if we assume that the CFF is also nearly periodic in nature, then we can say that maximum energy demand will appear at a specific point of the periodic signal with the net zero energy at the end of every period. This point actually helped us to find out the minimum head room required for SIR of SC during an CFF even without having specific information related to the CFF profile parameters. The only information required is the peak frequency fluctuation expected to be serviced. Based on this assumption, we can mathematically write the CFF as in (2).

$$CFF = F_{nom} + \Delta f_m cos(wt) \tag{2}$$

Where, F_{nom} is the nominal frequency and Δf_m is the peak fluctuation expected around its envelope as shown in Fig. 3(a).

Now the RoCoF can be calculated by differentiating (2) with respect to time as in (3).

$$\frac{df}{dt} = -w\Delta f_m sin(wt) \tag{3}$$

Similarly, the corresponding power demand can be expressed as in (4) [16].

$$P_{SIR} = -\frac{2HP_{nom}}{F_{nom}} w\Delta f_m sin(wt) \tag{4}$$

Where maximum power demand can be written as in (5).

$$P_m = \frac{2HP_{nom}}{F_{nom}} w\Delta f_m \tag{5}$$

Now, the energy during SIR can be calculated by integrating (4). But as our topic of concern is to find out the peak energy demand (E_m) only, the E_m will appear at the end of every quarter cycle of the power profile due to $\pi/2$ radian phase shifted as shown in Fig. 3(b) and can be calculated as in (6).

$$E_m = \int_0^{T/4} -\frac{2HP_{nom}}{F_{nom}} w\Delta f_m sin(wt)dt = \frac{2HP_{nom}}{F_{nom}} \Delta f_m \tag{6}$$

From (5), we can understand that E_m is a function of Δf_m only irrespective of the RoCoF and the frequency of fluctuation.

So just by the knowledge of the targeted Δf_m, one can calculate the maximum energy required for the SIR operation.

Considering the benchmark CFF parameters in Table. 1, the corresponding E_m can be calculated as $\approx 650\, jules$. Now, the maximum voltage required for SIR (V_{SIR}^{max}) with the essential headroom can be calculated using (7) and (8), which is derived from the basic energy expression of any capacitor.

$$E_m = \frac{1}{2} C_{SC}[(V_{SC}^{nom})^2 - (V_{SIR}^{max})^2] \tag{7}$$

$$V_{SIR}^{max} = \sqrt{V_{SC}^{nom^2} - \frac{2E_m}{C_{SC}}} \tag{8}$$

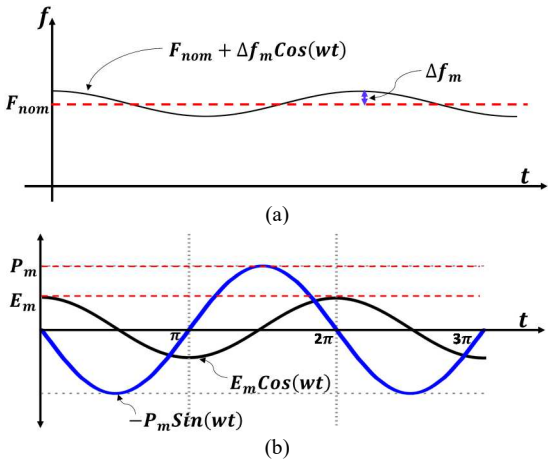

Fig. 3. The representation of a CFF waveform a per our assumption.

Now by using (8), and the parameters from Table. 2, the V_{SC}^{max} is calculated to be ≈ 47.3 V. That means the minimum headroom required below V_{SC}^{nom} is ≈ 0.7 V for our case.

Similarly, the minimum voltage set point required for an UFE $\left(V_{UFE}^{min}\right)$ can be estimated on considering the parameters from Table. 2 as ≈ 43 V.

Now, its in the hand of the user to set V_{SC}^{ss} as an intermediate value between V_{UFE}^{min} and V_{SIR}^{max}, which is here considered midway at 45 V.

V. Simulation and Results

This proposed concept is validated in simulations via MATLAB/Simulink for various case studies for SIR during CFF, UFE and OFE etc. and their results are shown in Fig. 4, 5 and 6 respectively.

A. Case Study for SIR

Here the PVS under consideration is subjected to a test case of CFF for the SIR parameters as mentioned in Table. 2 but for four different combination of initial V_{SC} (V_{SC0}) and Solar insolation (I_{rr}): (Case1: 45V, 1000W/m2; Case2: 45V, 400W/m2; Case3: 24V, 1000W/m2 and Case4: 24V, 400W/m2) and their results are shown in Fig. 4.

Observations from the simulation results for SIR:

- Fig. 4(b): Grid power is able to follow the fluctuations in SC power profile, irrespective of the V_{SC0} and I_{rr}.
- Fig. 4(b): Grid power profiles are a little dc shifted for Cases 3 & 4 due to the considerable effect of ΔP_{SC}^{Rec}. This is equivalent to slightly lower PV generation and does not cause any trouble.
- Fig. 4(c): ΔP_{SC}^{Rec} is very small for the Cases 1 & 2, however, for the Cases 3 & 4, is almost 250 W during starting and goes on decreasing as SC starts charging towards V_{SC}^{SS}.
- Fig. 4(d): For the Cases 1 & 2, the SC voltage profiles are quite stable due to almost negligible net energy exchange. However, the slow rising voltage profile in Cases 3 & 4 is only due to the support from the ΔP_{SC}^{Rec}.

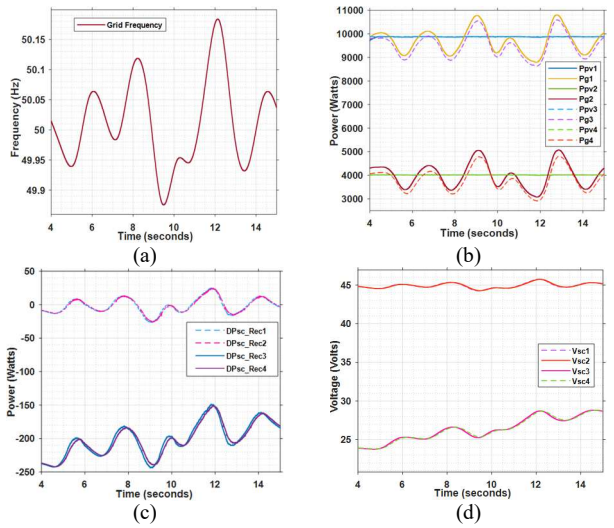

Fig. 4. Simulation results for SIR corresponding to four different cases of V_{SC0} and I_{rr} during CFF.

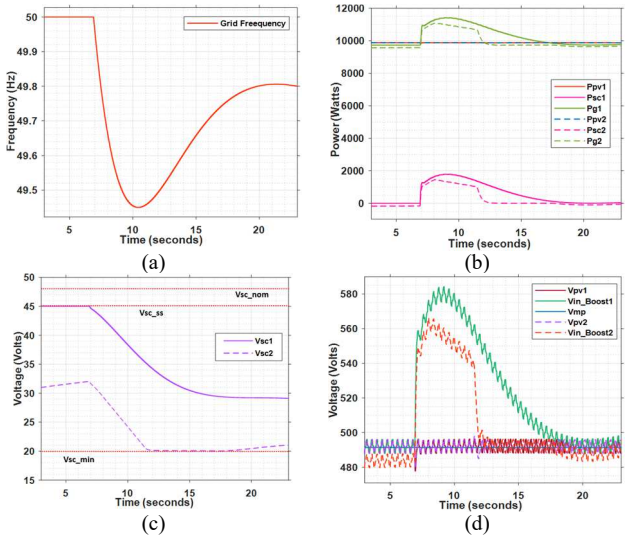

Fig. 5. Simulation results showing for PFR for an UFE corresponding to two different cases of V_{SC0}.

B. Case Study for PFR (UFE)

In this case, the PVS under consideration is subject to the benchmark UFE of Table I, but for two different cases of V_{SC0}: (Case 1: 30V; Case 2: 45V) to understand the capability and limitations of the PSCT during an UFE for the available SC storage capacity. The simulation results are shown in Fig. 5.

The main observations are:

- Fig. 5(b): SC is not able to follow the P_{SC}^{Ref} for Case 1 (Peak shaved) due to hitting the extreme limits like P_{SC}^{max} at time (t = 8 Sec) followed by the V_{SC}^{min} limit at (t = 11.5 Sec). Thanks to VPS, which comes into action in no time to clamp the SC voltage to V_{SC}^{min} as can be seen in Fig. 3(c). However, it is not the case with Case 2 as no bounds are hit.
- Fig. 5(c): For case 2, by the end of the event, the SC still left with 30 V ($\approx 40\%\ of\ its\ SOC$), sufficient enough to take care of another UFE back to back with similar/better performance shown for Case 1.
- Fig. 5(d): PV is exactly tracking the V_{mpp} for both Cases 1 & 2 irrespective of the situation (Decoupled from FRS). The V_{in} for the PV Boost converter can be seen adjusting based on the SC due to the cascaded nature of the converter.

C. Case Study for PFR (OFE)

In this case, the PVS under consideration is subject to the benchmark OFE of Table I, but for two different cases of V_{SC0}: (Case 1: 30V; Case 2: 45V) to understand how the proposed control switches between the PV MPPT mode and PV PCC mode when the SC hits its voltage and current limits during an OFE for the available SC storage capacity. The simulation results are shown in Fig. 6.

The main observations are:

- Fig. 6(b): SC is able to follow P_{SC}^{Ref} for Case 1, but peak shaved due to hitting the extreme limits like P_{SC}^{max} for the duration (t = 7.8 Sec to 9.3 Sec). However, for Case 2, the SC hits the V_{SC}^{nom} limit at (t = 8.3 Sec), awaking the voltage clamp control and finally seizing its output to zero but compensated by enabling the PV PCC.

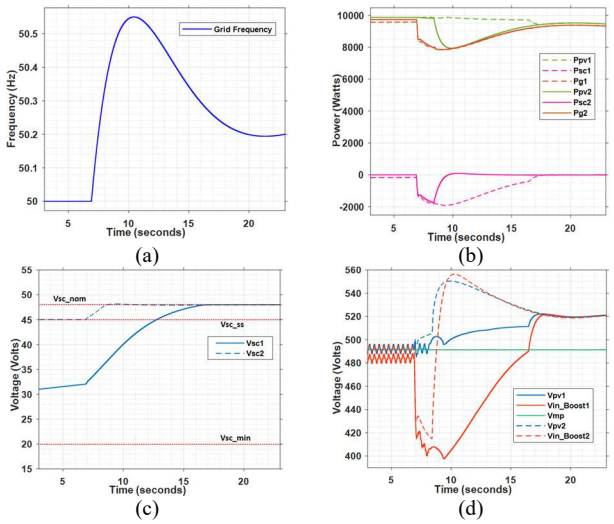

Fig. 6. Simulation results showing for PFR for an OFE corresponding to two different cases of V_{SC0}.

- Fig. 6(c): For case 1, the SC hits the V_{SC}^{nom} limit at (t = 16.5 Sec) before the end of the event completely, hence diverted the control to PV PCC mode, freezing the PV MPPT control.
- Fig. 6(d): *PV* is exactly tracking the V_{mpp} for both Cases 1 & 2 before the starting of the OFE at (t = 6.9 Sec). However, can be seen moving to PV PCC mode to meet the necessary compensated power demand whenever SC fails to achieve.

VI. CONCLUSION

This paper presents a complete Frequency Response Services scheme for a PVS by hybridizing SC storage with the PV curtailment control such that an optimal use of the available resources can be achieved. The advantages of PV curtailment control are explored by bringing it into action to assist the SC only for the duration when it the latter gets exhausted. As a result, PV is allowed for MPP extraction almost all the time unlike other PV derated controls presented in literature for FRS.

Nonetheless, a methodology is proposed to find a set point for the steady state operation of SC at any time by virtue of deciding the minimum headroom required for the SIR operation during continuous frequency fluctuation. It does not really need all the information of frequency fluctuation like RoCoF or frequency of variation, but just the peak value of oscillation. In addition to that, a zone wise control scheme is also proposed which not only helps in recovering the SC voltage to steady state but also helps in clamping it when its extreme limits are hit.

ACKNOWLEDGEMENT

This work was financially supported by DST, Govt. of India and EU's Horizon 2020 Research and Innovation Program through the RE-EMPOWERED Project under Grant Agreement No DST/TMD/INDIA/EU/ILES/2020/50(c) and 101018420 respectively, as well as by the Royal Academy of Engineering under the Engineering for Development Research Fellowship scheme (number RF\201819\18\86), Govt. of UK.

REFERENCES

[1] Capacity-and-Generation. Available online: https://www.irena.org/Statistics/View-Data-by-Topic/Capacity-and-Generation (accessed on 2 July 2020)

[2] R. Rajan, M. F. Francis, Y. Yang, "Primary frequency control techniques for large-scale PV-integrated power systems: A review," Renew. Sustain. Energy Rev. vol. 144, pp. 1364–0321, 2021.

[3] B. Hartmann, I. Vokony, I. Táczi, "Effects of decreasing synchronous inertia on power system dynamics—Overview of recent experiences and marketisation of services," Int. Trans. Electr. Energy Syst., 29, 2019.

[4] Black System South Australia 28 September 2016—Final Report. Available online: http://www.aemo.com.au/-/media/Files/Electricity/NEM/Market_Notices_and_Events/Power_System_Incident_Reports/2017/Integrated-Final-Report-SA-Black-System-28-September-2016.pdf (accessed on 12 July 2021).

[5] H. Ibrahim, A. Ilinca, J. Perron, "Energy storage systems—Characteristics and comparisons," Renew. Sustain. Energy Rev., vol. 12, pp. 1221–1250, 2008.

[6] K. Tam, P. Kumar, M. Foreman, "Enhancing the utilization of photovoltaic power generation by superconductive magnetic energy storage," IEEE Trans. Energy Convers., vol. 4, pp. 314–321, 1989.

[7] D. Sutanto, K. W. E. Cheng, "Superconducting magnetic energy storage systems for power system applications," In Proceedings of the International Conference on Applied Superconductivity and Electromagnetic Devices, Chengdu, China, 25–27 September 2009.

[8] G. Delille, B. François, G. Malarange, "Dynamic frequency control support: A virtual inertia provided by distributed energy storage to isolated power systems," In Proceedings of the 2010 IEEE PES Innovative Smart Grid Technologies Conference Europe (ISGT Europe), Gothenburg, Sweden, pp. 1–8, 11–13 October 2010.

[9] M. M. Agha, A. Hajar, "A new approach for optimal sizing of battery energy storage system for primary frequency control of islanded Microgrid," Int. J. Electr. Power Energy Syst., vol. 54, pp. 325–333, 2014.

[10] D. Lee, L. Wang, "Small-Signal Stability Analysis of an Autonomous Hybrid Renewable Energy Power Generation/Energy Stor-age System Part I: Time-Domain Simulations," IEEE Trans. Energy Convers., vol. 23, pp. 311–320, 2008.

[11] P. C. Sekhar, S. Mishra, "Storage Free Smart Energy Management for Frequency Control in a Diesel-PV-Fuel Cell-Based Hybrid AC Microgrid," IEEE Trans. Neural Netw. Learn. Syst., vol. 27, pp. 1657–1671, 2016.

[12] D. Bazargan, B. Bahrani, S. Filizadeh, "Reduced Capacitance Battery Storage DC-Link Voltage Regulation and Dynamic Im-provement Using a Feedforward Control Strategy," IEEE Trans. Energy Convers., vol. 33, pp. 1659–1668, 2018.

[13] K. Guo, Y. Tang, J. Fang, "Exploration of the Relationship Between Inertia Enhancement and DC-Link Capacitance for Grid-Connected Converters," In Proceedings of the IEEE 4th Southern Power Electronics Conference (SPEC), Singapore, 10–13 De-cember 2018.

[14] M. Jami, Q. Shafiee, M. Gholami, B. Hassan, "Control of a super-capacitor energy storage system to mimic inertia and transient response improvement of a direct current micro-grid," J. Energy Storage, vol. 32, pp. 101788, 2020.

[15] T. Monai, I. Takano, H. Nishikawa, Y. Sawada, "A collaborative operation method between new energy-type dispersed power supply and EDLC," IEEE Trans. Energy Convers., vol. 19, pp. 590–598, 2004.

[16] S. Karpana, E. Batzelis, S. Maiti, C. Chakraborty, "PV-Supercapacitor Cascaded Topology for Primary Frequency Responses and Dynamic Inertia Emulation," Energies, vol. 14. pp. 8347, 2021.

[17] A. Sangwongwanich, Y. Yang, F. Blaabjerg, D. Sera, "Delta Power Control Strategy for Multistring Grid-Connected PV Invert-ers," IEEE Trans. Ind. Appl., vol. 53, pp. 3862–3870, 2017.

[18] E. I. Batzelis, G. Anagnostou, I. R. Cole, T. R. Betts and B. C. Pal, "A State-Space Dynamic Model for Photovoltaic Systems With Full Ancillary Services Support," in IEEE Transactions on Sustainable Energy, vol. 10, no. 3, pp. 1399-1409, July 2019.

[19] P. P. Zarina, S. Mishra, P. C. Sekhar, "Exploring frequency control capability of a PV system in a hybrid PV-rotating machine-without storage system," Int. J. Electr. Power Energy Syst., vol. 60, pp. 258–267, 2014.

[20] B. Pawar, S. Chakrabarti, E. I. Batzelis and B. C. Pal, "Grid-Forming Control for Solar PV Systems with Real-Time MPP Estimation," 2021 IEEE Power & Energy Society General Meeting (PESGM), 2021.